Computers and Mathematics with Applications 56 (2008) 1291–1302

Contents lists available at ScienceDirect

Computers and Mathematics with Applications

journal homepage: www.elsevier.com/locate/camwa

Comparison and validation of multi phase closure models☆

W. Bo [a], H. Jin [b], D. Kim [a], X. Liu [a], H. Lee [a], N. Pestieau [a], Y. Yu [a], J. Glimm [a,c], J.W. Grove [d,*]

[a] *Department of Applied Mathematics and Statistics, Stony Brook University, Stony Brook, NY 11794-3600, USA*

[b] *Department of Mathematics, Cheju National University, Jeju, 690-756, Republic of Korea*

[c] *Computational Science Center, Brookhaven National Laboratory, Upton, NY 11793-6000, USA*

[d] *Continuum Dynamics Group, Computer, Computational, and Statistical Sciences Division, Mail Stop D413, Los Alamos National Laboratory, Los Alamos, NM 87545, USA*

ARTICLE INFO

Article history:
Received 3 January 2008
Accepted 6 February 2008

Keywords:
Multiphase flow
Closure
Turbulence

ABSTRACT

The purpose of this paper is to propose a simple (one or two parameter) multiphase flow model, suitable for the description of Rayleigh–Taylor and Richtmyer–Meshkov mixing layers. We justify model closure assumptions in this model by comparison to Rayleigh–Taylor and Richtmyer–Meshkov simulation data. We show that the relative errors related to model closure terms are about 10%, and are about two to four times smaller than related closure models of Abgrall and Saurel.

1. Introduction

We are concerned with acceleration driven turbulent mixing. This is an interesting and complicated problem which has attracted the attention of prominent physicists and mathematicians over many decades [1–3]. As with turbulence modeling (of a single fluid), numerical studies of the turbulent mixing of multiple fluids often proceed at three levels of detail, each proposed for different types of studies. Full resolution of all length scales is called direct numerical simulation (DNS), and is practical only for small scale problems. Averaging of all equations, to obtain differential equations for mean flow quantities is called Reynolds Averaged Navier–Stokes simulations (RANS). In this approach, all of the turbulent fluctuations and much of the flow detail is suppressed. Our main concern is a two phase version of this approach. Intermediate between DNS and RANS is large eddy simulation (LES). In LES, the larger of the turbulent and fluctuating scales are resolved, while the smaller ones lie below the grid scale and are not resolved. We use two phase LES to provide validation data to assess closure terms in the two phase RANS model we propose. These LES, which do not include closure terms to express the influence of the missing small scales upon the dynamics of the large scales, are known as implicit LES (ILES).

The key difficulty for RANS is the averaging of the nonlinear terms in the flow equations, a process which introduces new unknowns. To obtain a closed, and thus solvable, set of equations, the averages of the nonlinear terms must be approximated in some sense by expressions involving averages of the (primitive) variables of original equations. Distinct models are defined by different approximations, called closures, and the quality of the models is assessed by the accuracy of the closures, or by the accuracy of the RANS which the closures define. Here assessment is measured in the context of LES for Rayleigh–Taylor (RT) and Richtmyer–Meshkov (RM) unstable mixing flows.

☆ This work was supported in part by the US Department of Energy, US Department of Energy grants DE-AC02-98CH10886 and DE-FG52-06NA26208, and the Army Research Office grant W911NF0510413. Los Alamos National Laboratory preprint number LA-UR-07-1964. The second author was supported in part by a Korea Science and Engineering Foundation (KOSEF) grant funded by the Korean government (MOST) (No. R01-2007-000-11443-0).

* Corresponding author.
E-mail address: jgrove@lanl.gov (J.W. Grove).

0898-1221/$ – see front matter © 2008 Elsevier Ltd. All rights reserved.
doi:10.1016/j.camwa.2008.02.030

We begin with a buoyancy–drag equation [4]

$$(-1)^k \ddot{Z}_k = Ag - C_k^d \frac{1-(-1)^k A}{2} \frac{V_k^2}{|Z_k|}. \tag{1.1}$$

to predict the location of the edges $Z_k(t)$ of the mixing zone for RT and RM instabilities. Related equations have been considered by a number of authors [5,6]. Here $A = (\rho_2 - \rho_1)/(\rho_1 + \rho_2)$ is the Atwood number and $k = 1$ (light fluid) and 2 (heavy fluid). To predict mixing zone growth for most RT and RM data, two adjustable parameters are required [7,4]: the bubble side RT drag coefficient C_1^d for Atwood numbers $A \le 0.8$ and a second parameter C_2^d to improve the description of the Atwood number dependence of the spike side drag. C_2^d is expressed in terms of C_1^d according to the analysis of Cheng et al. [8]. The model fits available data for all A, $0 \le A \le 1$.

The models proposed here were derived by a conventional averaging process, starting with the multifluid equations. We average the compressible Euler or Navier–Stokes equations. In contrast to many such multiphase models, we retain averages of all primitive variables and independent thermodynamics for each phase. Specifically, each phase has its own pressure and temperature. In practice, the pressures are close to equilibration, but by not imposing this equality as an identity, we avoid some complications of mixed phase thermodynamics and we avoid issues of hyperbolic instability in the averaged equations, which would lead to a non-physical phase separation [9]. The model equations use (1.1) to supply an otherwise missing equation at the mixing zone boundaries, and they require models for closure resulting from averages of nonlinear terms. Models for the closures have been proposed by a number of authors. Representative examples of such models have been surveyed by Cheng [10]. The main point of the present paper is to show that the result is insensitive to all parameters in the closure proposed here so that they can be eliminated from the model or are constrained from (1.1). Thus the model for the mixing zone interior has no adjustable parameters, beyond those required for (1.1).

To arrive at this conclusion, we compare closure terms for two fluid RT and RM simulation data. We find average relative errors in the closures at about 10%. Closures in a related model of Abgrall and Saurel have relative errors about two or four times larger.

2. The primitive and the averaged equations

In the present paper, we assume that the edge motions have been determined, for example by (1.1) or some suitable generalization of this equation. We have found sensitivity of the edge motions Z_k to transport and other scale breaking effects [11,12], but a main conclusion of the present paper is that the closure terms for the averaged equations in the mixing zone interior are insensitive to such effects. For simplicity, we drop such terms from the primitive equations, and start with the two fluid compressible Euler equations as the primitive equations. The coupling of the edge motions to the interior can be expressed mathematically as supplying a missing boundary condition at each edge in order to replace incoming characteristics from a phase which does not exist in a single phase region. The numerical implementation of this concept is given in [13]. The insensitivity of this information to the interior flow comes from the fact that the main effects are already included via this coupling. For details, see [14]. For simplicity, we formulate the equations in terms of two phases. See Cheng et al. [15] for extensions of the equations below to the general multiphase case, in the incompressible limit. Let the function X_k be the phase indicator for material $k (k = 1, 2)$; *i.e.*, $X_k(t, \mathbf{x})$ equals 1 if position $\mathbf{x}$ is in phase k at time t, zero otherwise. For immiscible fluids, the presence of a sharp interface ∂X_k between the fluids gives a well defined meaning to the phase indicator function X_k. For miscible fluids, X_k is a useful approximation tool, but only for times which are small relative to the diffusion process between the fluids. In this case, we can regard the boundary ∂X_k of X_k as representing the mean location or the 50% level set of the species concentration function within a narrow diffusive mixing zone that characterizes the transition between distinct species concentrations. Within each phase, there is a single fluid velocity, while across phase boundaries (at the microphysics level, i.e. before averaging), the distinct phase velocities have continuous normal components.

We average the advection law

$$\frac{\partial X_k}{\partial t} + \mathbf{v}_{\text{int}} \cdot \nabla X_k = 0 \tag{2.1}$$

for the indicator function X_k of the region occupied by the fluid k, with derivatives considered in the distributional sense. A derivation of (2.1) can be found in the article of Drew [16]. Corrections to this formula to allow for small amounts of mass diffusion is one of many complicating details that turn out not to matter for the present purpose, namely assessing accuracy of closures for the interior of the mixing zone. These terms are thus omitted in the interests of simplicity.

Multiphase equations for the phase k are obtained by multiplying the primitive equations [17] by X_k and performing an ensemble average, following the ideas of Drew [16]. Typically we consider averaged equations depending on fewer independent variables than time plus the three variables of physical space. The ensemble to be averaged is assumed to be independent of the missing variables. Thus in a rectangular coordinate system, we assume the ensemble is independent of x or of x and y. The ensemble average in this case includes an average over the suppressed spatial variables. We also want to allow statistical ensembles possessing cylindrical or spherical symmetry, for which purpose we introduce the geometry indicator s, $s = 0, 1, 2$ corresponding to the planar, cylindrical and spherical form of the primitive equations. In rectangular coordinates, we integrate the equations over the x or x and y directions. In cylindrical coordinates, we integrate the equations

over the θ or θ and z directions, in spherical coordinates, we integrate the equations over the θ or θ and ϕ directions. This yields one or two dimensional multi-phase flow averaged equations. When the equations are given in cylindrical and spherical coordinates, there are geometrical source terms due to the curvilinearity of the coordinate systems. See Malvern's book [17] for details.

In fact, this picture is a simplification. In a more general context, not developed in detail here, the variables are reduced locally, with a single preferred direction normal to the mixing layer, determined locally by the flow field, and two other directions locally tangent to it. Often, one or both of those tangent directions will be averaged over, but in any case the single normal direction will play a dominant role. In the present study, this mixing layer normal direction is fixed globally to be the z or the r direction.

The averaging operator $\langle\cdots\rangle$ in the present paper is exclusively a global average over suppressed variables, but more generally it may also be a local spatial or space time average or an ensemble average over some ensemble of statistically equivalent simulations. For many situations, these averages are all equivalent, but where they differ, it is necessary to be precise which is being used.

The average of the indicator function X_k is denoted $\beta_k \equiv \langle X_k\rangle$; $\beta_k(z,t)$ is then the expected fraction of the horizontal layer at height z that is occupied by fluid k at time t. Averaging removes most discontinuities from the solution. Specifically, although X_k is discontinuous, β_k will usually be continuous.

For other variables, we use two types of averaging. The phase average of a variable f is defined by

$$f_k = \langle X_k f\rangle / \beta_k, \tag{2.2}$$

and the phase mass-weighted average is defined as

$$f_k = \langle X_k \rho f\rangle / \langle X_k \rho\rangle . \tag{2.3}$$

In the averaged equations, only two variables, the averaged velocities and the averaged total energy, are defined by the phase mass-weighted average (2.3). For later use, we also consider a mass weighted entropy and internal energy. All other averaged variables are defined by the phase average (2.2).

In the remainder of this paper, we choose a preferred direction normal to the mixing layer and integrate the primitive equations over two other directions tangent to it. This procedure yields one dimensional averaged equations. We follow Drew [16] and earlier papers in the present series [18–20] to obtain

$$\frac{\partial \beta_k}{\partial t} + v^* \frac{\partial \beta_k}{\partial z} = 0, \tag{2.4}$$

$$\frac{\partial(\beta_k \rho_{ki})}{\partial t} + \nabla^s(\beta_k \rho_{ki} v_k) = \beta_k \mathcal{D}_{ki}, \tag{2.5}$$

$$\frac{\partial(\beta_k \rho_k v_k)}{\partial t} + \nabla^s(\beta_k \rho_k v_k^2) = -\frac{\partial}{\partial z}(\beta_k p_k) + p_k^* \frac{\partial \beta_k}{\partial z} + \beta_k \rho_k g + \beta_k \mathcal{M}_k, \tag{2.6}$$

$$\frac{\partial(\beta_k \rho_k E_k)}{\partial t} + \nabla^s(\beta_k \rho_k v_k E_k) = -\nabla^s(\beta_k p_k v_k) + (p_k v)^* \frac{\partial \beta_k}{\partial z} + \beta_k \rho_k v_k g + \beta_k \mathcal{E}_k. \tag{2.7}$$

Summing the Eq. (2.5) over i, we get the equations for total mass

$$\frac{\partial(\beta_k \rho_k)}{\partial t} + \nabla^s(\beta_k \rho_k v_k) = 0, \tag{2.8}$$

where

$$\nabla^s f(z) = \frac{1}{z^s} \frac{\partial z^s f(z)}{\partial z} \tag{2.9}$$

is the curvilinear divergence. For convenience, we use the following symbols to represent the source terms of (2.5)–(2.7)

$$\mathcal{D}_{ki} = (\nabla \cdot \mathbf{j}_i)_k \tag{2.10}$$

$$\mathcal{M}_k = (\nabla \cdot \boldsymbol{\tau}')_{k,3} + f_k^s, \tag{2.11}$$

$$\mathcal{E}_k = (\nabla \cdot \boldsymbol{\tau}' \mathbf{v})_k + \left(\nabla \cdot \left(\sum_i h_i \mathbf{j}_i\right)\right)_k + (\nabla \cdot (\kappa \nabla T))_k, \tag{2.12}$$

in which τ' is the viscous stress tensor, f_k^s is the averaged geometrical source term; $f_k^s = 0$ for rectangular coordinates [17]. h_i is the specific enthalpy of species i, $\mathbf{j}_i$ is the diffusion flux [21]. κ is the heat conductivity. $(\nabla \cdot \boldsymbol{\tau}')_{k,3}$, and v_3 mean the third component of $(\nabla \cdot \boldsymbol{\tau}')_k$ and $\mathbf{v}$. Therefore, the source terms $\mathcal{D}_{ki}$, $\mathcal{M}_k$, and $\mathcal{E}_k$ represent the effects of mass diffusion, viscosity and heat conduction, as well as geometrical source terms. As described in Section 3, some of these effects are present in the simulation data. We have found sensitivity of the edge motion, $Z_k(t)$, to such terms. An important conclusion of this paper is that these effects are negligible in the models for the closure in the interior of the mixing zone. To simplify the discussion, they are henceforth set to zero.

The Reynolds stress relating to the combined phases is large, the effect of this term is included within the model equations. In contrast, turbulence within a single phase is typically much smaller, and on this basis we neglect the in phase Reynolds stress. Stated alternatively, the velocity differences between the heavy and light fluids are large, and the associated Reynolds stress is already present in the equations. The velocity fluctuation within a light or heavy fluid bubble or droplet is small and can be neglected in the averaged equations, that is to say for example, we are taking advantage of the fact that the light fluid velocity fluctuations about the light fluid mean velocity are small. Also, v^*, p_k^*, $(p_k v)^*$ are the averaged quantities at the interface

$$v^* = \frac{\langle \mathbf{v} \cdot \nabla X_k \rangle}{\langle \mathbf{n}_3 \cdot \nabla X_k \rangle}, \qquad p_k^* = \frac{\langle p_k \mathbf{n}_3 \cdot \nabla X_k \rangle}{\langle \mathbf{n}_3 \cdot \nabla X_k \rangle}, \qquad (p_k v)^* = \frac{\langle p_k \mathbf{v} \cdot \nabla X_k \rangle}{\langle \mathbf{n}_3 \cdot \nabla X_k \rangle}, \tag{2.13}$$

where $\mathbf{n}_3$ is the unit normal vector in the preferred direction. Although the Eq. (2.13) allow multiple fluids, they only allow a single interface type, i.e. at most two fluid phases. A generalization [15] of this framework to multiple phases specifies an interface type for each pair of phases that are in contact, and leads to a generalization of the system (2.13).

The definitions (2.13) are fundamental to all that follows. They are mathematically exact consequences of the averages of the primitive equations and specify the quantities (the right hand side of (2.13)) that are to be approximated in a definition of closure to complete the averaged Eqs. (2.4)–(2.7).

Note that ∇X_k equals the unit normal to the boundary ∂X_k times a delta function concentrated on ∂X_k. The definitions assume that interface fluxes weighted by this vector measure are proportional to fluxes through the z direction only. Also for an interface quantity such as p^*, which may be discontinuous across the interface (due to surface tension), the notation p_k^* indicates evaluation from the interior X_k side of ∂X_k.

3. Simulation data for assessment of closure

We explain the simulation data sets used to assess errors in the closure terms. The simulation method, in the language of turbulence models, is implicitly filtered LES. In the language of numerical analysis, it is a higher order Godunov method, with a front tracking capability. With use of front tracking, the numerical mass diffusion across the surface is very small, and Schmidt numbers(viscosity divided by diffusivity) over a large range can be simulated effectively.

We will consider four classes of simulations of the mixing process. The first is an ideal simulation of three dimensional Rayleigh–Taylor multimode mixing [11]. This simulation has no surface tension, no mass diffusion, no viscosity (other than numerical viscosity) and no thermal conductivity. The second class of simulations is a modification of the former, with three different values of dimensionless surface tension [11]. These simulations span the experimental range of dimensionless surface tensions found in the Rayleigh–Taylor experiments of Reed [22] and Smeeton–Youngs [23] for all of their experiments with immiscible fluids and no surfactants. The mixing rate α_b found from these simulations is in agreement with the above experiments.

The third class of simulation models, of the Banerjee–Andrews air–helium RT experiments [24], has physical values of mass diffusion dimensionalized using an initial wave length $\lambda = 0.5$ cm set from observation of the flow [12]. The viscosity is small in comparison to the mass diffusion, and is modeled as zero. There is no surface tension. These simulations are also in agreement with experiment.

These three classes of simulations used a gamma law gas. The simulations are nearly incompressible and so EOS issues are not of major importance. We used $\gamma = 5/3$. They were performed using a grid resolution of $128^2 \times 512$. Periodic boundary conditions were used in the x and y directions, while free slip Neumann boundaries were imposed in the z direction. These simulations reach a dimensionless time comparable to that of the alpha group study [25], with fewer modes and with double the mesh resolution per mode. Consistent with the analysis of Cabot and Cook [26], we reexamined the definitions of α used in these simulations. We had previously used definitions based on h (not favored by Cabot and Cook) and on $\ddot{h}$. We had found consistency between these definitions, and on replotting with the $\dot{h}$ definition [26], we found near identity with our $\ddot{h}$ analysis.

Our final class of direct simulation data is a previously studied [27] circular 2 dimensional Richtmyer–Meshkov unstable data set. The problem has a single interface separating an exterior heavy fluid (tin) and an interior light fluid (plastic) separated by a perturbed circular interface and subject to a strong inward moving circular shock. Both materials were modeled by stiffened gamma law gasses [28]. Surface tension, viscosity, and mass diffusion were modeled as zero. The time period studied includes the first shock passage through the interface, reflection of this shock at the origin, reshock of the interface by the reflected shock wave, and subsequent evolution of the mixing zone. A variety of grids were used, with the finest (800×1600) used for the collection of averaged data.

4. Two closures

Here we explain the basic ideas of our proposed closures, and their relation to the closures of Saurel and coworkers [29–31]. There are three terms to define in (2.13), v^*, p^*, $(pv)^*$, the interface averages of p, v, pv, which we denote generically as q^*, $q = v, p, pv$. For the Saurel et al. closed equations, these same quantities are also required (and have different definitions). Their equations contain additional terms called relaxation terms.

We assume a closure which represents q^* as a convex sum of the primitive variables q_k for $q = v, p$,

$$q^* = \mu_1^q q_2 + \mu_2^q q_1, \quad q = v, p \tag{4.1}$$

and a related bilinear expression

$$(pv)^* = p^*(\mu_1^{pv} v_2 + \mu_2^{pv} v_1) + v^*(\mu_1^{pv} p_2 + \mu_2^{pv} p_1) - (\mu_1^{pv} p_2 v_2 + \mu_2^{pv} p_1 v_1) \tag{4.2}$$

for $(pv)^*$.

Saurel et al. employ a related but different functional form for their closure. They also consider a convex sum

$$q'^{S*} = \mu_1^{Sq} q_2 + \mu_2^{Sq} q_1 \quad q = v, p, \tag{4.3}$$

and then define

$$v^{S*} = v'^{S*} + \operatorname{sgn}\left(\frac{\partial \beta_1}{\partial x}\right) \frac{p_2 - p_1}{\mathcal{Z}_1 + \mathcal{Z}_2}, \tag{4.4}$$

$$p^{S*} = p'^{S*} + \operatorname{sgn}\left(\frac{\partial \beta_1}{\partial z}\right) \left(\frac{\mathcal{Z}_1 \mathcal{Z}_2}{\mathcal{Z}_1 + \mathcal{Z}_2}\right) (v_2 - v_1). \tag{4.5}$$

Here $\mathcal{Z}_k$ is the acoustic impedance of fluid k. We interpret the second terms in (4.4) and (4.5) as two relaxation terms for the closures. Also

$$(pv)^{S*} = p^{S*} v^{S*}. \tag{4.6}$$

The Saurel closures also include relaxation terms for their equations, as an additional term in the RHS of the associated volume fraction, momentum and energy equations. These terms (for $k = 1$) have the form:

$$\mu^S (p_1 - p_2) \quad \text{volume fraction source term} \tag{4.7}$$

$$\lambda^S (v_2 - v_1) \quad \text{momentum source term} \tag{4.8}$$

$$\lambda^S v'^{S*} (v_2 - v_1) - \mu^S p'^{S*} (p_1 - p_2) \quad \text{energy source term.} \tag{4.9}$$

Here

$$\mu^S = \frac{A_I}{2(\mathcal{Z}_1 + \mathcal{Z}_2)}, \qquad \lambda^S = \mu \mathcal{Z}_1 \mathcal{Z}_2, \tag{4.10}$$

where A_I is the interfacial area per unit volume.

The convex coefficients μ_k^q and μ_k^{Sq} have a fractional linear form, namely

$$\mu_k^q = \frac{\beta_k}{\beta_k + d_k^q \beta_{k'}}, \quad q = v, p, pv \tag{4.11}$$

$$\mu_k^{Sq} = \frac{1}{1 + d_k^{Sq}}, \quad q = v, p. \tag{4.12}$$

The μ_k^q and μ_k^{Sq} thus depend on a single parameter d_k^q or d_k^{Sq}. The form of the μ_k^q is suggested by rewriting the exact equations to derive [32,33] an exact (unclosed) expression for q^* and μ_k^q. The form (4.11) of μ_k^q is motivated by these expressions as well and is, moreover, required by theoretically required boundary conditions at the edges of the mixing zone,

$$q^* = q_k \quad \text{at } z = Z_k. \tag{4.13}$$

Our closures satisfy (4.13). d_k^q is an adjustable parameter and will be determined by our LES simulation. With one exception, the accuracy of the model is insensitive to the choice of d_k^q. We set these d_k^q to 1 for definiteness. See Table 1. For the RT case, we assume $(-1)^k V_k = (-1)^k \dot{Z}_k \geq 0$ so that the mixing zone is expanding. The growing mixing zone entrains pure phase fluid into the mixture, and thus creates mixed fluid volume for both phases. In the incompressible, non-diffusive RT case, this is seen clearly from the closed form solution [34]

$$d_k^v(t) = \left(\frac{Z_{k'}}{Z_k}\right)^s \left|\frac{V_{k'}}{V_k}\right|. \tag{4.14}$$

The solution (4.14) is a consequence of the closed form expression obtained for the solution of the model equations and a simple calculation. See references of Glimm, Sharp and Saltz [35,34,36] for details of the derivation. In the planar case ($s = 0$), the ratio in (4.14) is a function of the Atwood number $A = (\rho_2 - \rho_1)/(\rho_2 + \rho_1)$, and can be determined exactly on the basis of a theory [8,7] which has been validated against experiments. For the data (Atwood number) considered here, (4.14) has the value 1.5.

The hyperbolic character of the resulting model equations is easily derived. At the edges of the mixing zone, the hyperbolic analysis detects a missing incoming characteristic from the single fluid side. We supply this missing condition by coupling

Table 1
Summary of d_k^q parameter choices for RT and RM mixing

	RT	RM
d_1^v	(4.14)	1.0
d_1^p	1.0	1.0
d_1^{pv}	1.0	1.0

All choices except that for d_k^v in the RT case are insensitive.

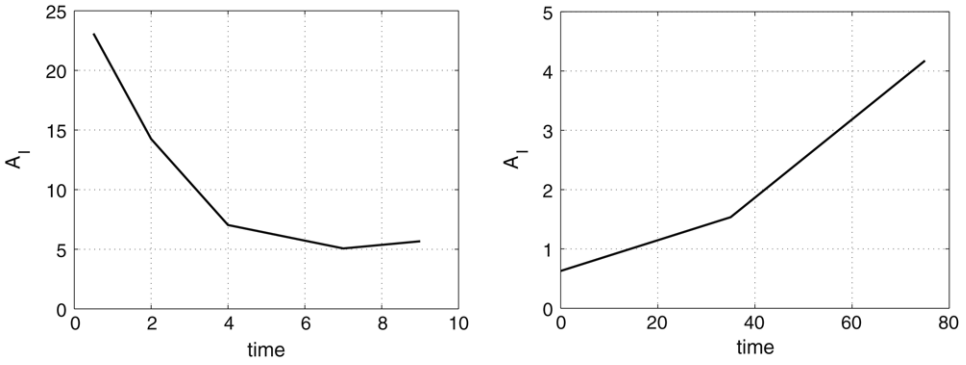

Fig. 1. The interfacial area A_I per unit volume plotted vs. time. This plot serves to define the parameter A_I for the closure Saurel-2. Left: RT, Right: RM.

the model at the mixing zone edges to the buoyancy drag Eq. (1.1). This analysis is needed as part of a direct solution of the model equations [13].

We see that the simple choice (4.14) for d_k^v depends on the buoyancy–drag equations for the mixing zone edge position Z_k. This equation has a free drag parameter which can be set by appeal to a bubble merger model [37], and to a model to set the ratio of bubble to spike growth rates [7]. This range of issues have also been discussed for compressible mixing [38]. In fact, our study of highly compressible RT mixing [39] shows that the self similar scaling law for RT mixing (and thus the buoyancy drag equation, which allows a self similar solution) remain valid in the deeply compressible region. To achieve this result it is necessary to use time dependent Atwood numbers, reflecting the differing densities in a stratified highly compressible atmosphere. We predict a strong increase in the mixing rate α with compressibility in this sense.

The Saurel et al. expressions,

$$d_k^{Sv} = Z_k/Z_{k\prime} \qquad d_k^{Sp} = Z_{k\prime}/Z_k, \tag{4.15}$$

are derived from solutions of approximate (linearized) Riemann problems modeling multiphase flows at the sub-grid level; their closure does not satisfy (4.13). The Saurel et al. model supplies the missing internal boundary conditions at the edges of the mixing zone by imposition of equal pressures [29] $p_1(z = Z_k) = p_2(z = Z_k)$.

We have two interpretations of the Saurel et al. model. In the first, which we denote as Saurel-1, A_I is regarded as a fitting parameter. The second interpretation of their model is to take advantage of the fact that A_I is a computed quantity in our data, and to use this time dependent value in the definition of the model. We denote this model as Saurel-2. A_I is plotted as a function of time in Fig. 1, to complete the definition of the Saurel-2 closure. We note that A_I has the dimensions of an inverse length and takes on large values at early time as the mixing layer tends to its (small) initial amplitude.

5. Closures: Overview of comparison

In Sections 6–8 we compare our closure, the two Saurel et al. closures and the RT or RM simulation data. In comparison to simulation data, we use the definition

$$\text{relative error} = \frac{1}{3}\sum_{v^*,p^*,(pv)^*} \frac{\iint |\text{data} - \text{model}|\, \text{d}z\text{d}t}{\iint |\text{data}|\text{d}z\text{d}t} \tag{5.1}$$

for the sum of the relative model errors for v^*, p^* and $(pv)^*$. The integration extends over the mixing zone. In the RT case, we exclude early time, before the bubbles have had much of a chance to interact, and to which the model is not supposed to apply, and integrate (i.e. sum) over times from 4 to 10.

Our first main conclusion is the excellent (about 10%) agreement of our closures with the simulation data.

Our second main conclusion is the comparison of our closure to Saurel et al. We have introduced in Section 4 two distinct interpretations of the Saurel et al. model. In Fig. 2, we show the dependence of the total relative error on the value assumed for the area A_I. The error is minimized for $A_I = 0$ for both the RT data and the RM data, defining two different Saurel et al. closures for these two data sets. With that choice, we compare the total relative errors in our model and the two Saurel

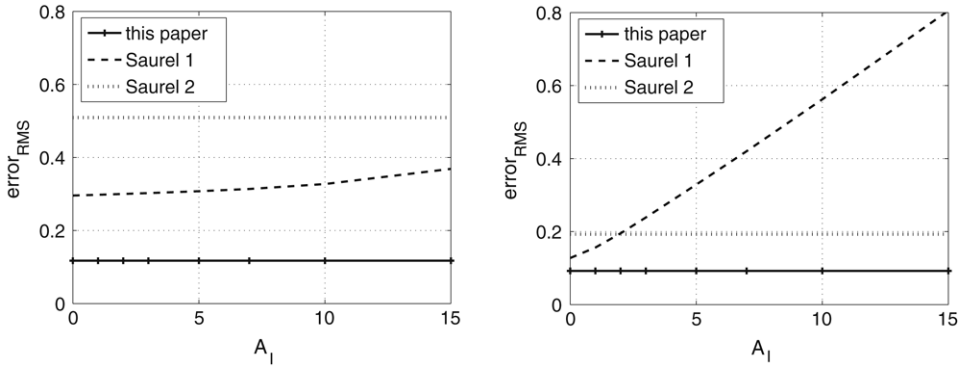

Fig. 2. Comparison of the model error (5.1) for three closures. Of these, only Saurel-1 depends on the value of A_I as a fitting parameter; these plots serve to locate the best fit value of A_I ($A_I = 0$) and thus to define the Saurel-1 closure. Left: RT, Right: RM.

Table 2
Model errors based on comparison to simulation data

Closure	v^*(%)	p^*(%)	$(pv)^*$(%)	Average(%)
		Comparison to RT data		
This paper	18	00	18	12
Saurel-1	43	02	42	30
Saurel-2	56	46	51	51
		Comparison to RM data		
This paper	07	00	20	09
Saurel-1	13	04	22	13
Saurel-2	12	15	31	19

Table 3
Summary properties related to the closures q^*

	v^*	p^*	$(pv)^*$
RT: Closure sensitive to d_k^q ((5.2) or (5.3) invalid)	Yes	No	No
RT: Closure sensitive to v^*	–	–	Yes
RT: Relaxation important	No	Late time	Late time
RM: Closure sensitive ((5.2) or (5.3) invalid)	No	No	No
RM: Relaxation important	No	Early time	Early time

It is remarkable that the closures depend sensitively on their defining parameter d_k^q only in the case of the RT data for the v^* closure.

models, see Table 2. In summary, our model has errors about one quarter to one half the size of those for the Saurel et al. model.

Our third main conclusion is the high degree of insensitivity of the q^* to the defining quantities μ_k^q, for many cases. We consider the condition

$$|\Delta q| \equiv |q_1 - q_2| \ll |\overline{q}| \equiv |\beta_1 q_1 + \beta_2 q_2| \quad q = v, p. \tag{5.2}$$

When (5.2) holds, q^* is effectively independent of the convex coefficients μ_k^q and thus of the value of q_k, as can be shown. This is the case for all RM data, $q^* = v^*$, p^*, and for p^* in the RT data. Moreover, $(pv)^*$ is insensitive to d_k^{pv} whenever (5.2) holds for $q = p$, which occurs for both RT and RM data, and in this case

$$(pv)^* \approx p^* v^*. \tag{5.3}$$

For these cases, the agreement of the two models and their agreement with the simulation data is understandable, but not a stringent test of the models. The insensitivity allows a simple choice of d_k^q, in cases where (5.2) holds. The only case where (5.2) is invalid is the v^* case for the RT instability. For the RT instability, v_1 and v_2 have generally opposite signs (in the frame stationary with the fluid container), so that $|\overline{v}|$ is small relative to $|\Delta v|$.

Our fourth main conclusion concerns the cases which violate (5.2), and thus for which the data is a stringent test of the models. This occurs for the v^* closure for the RT data. We find that our μ_k^v and those of Saurel et al. are significantly different.

The summary results of Table 3 can be understood as follows. The sensitive case for (5.2) occurs for the RT v^* closure only. In this case, the computational frame is that of the average interface position. The light fluid moves away from the direction of g and the heavy fluid moves in the direction of g. Thus in most parts of the mixing zone, v_1 and v_2 has opposite signs, so that $\overline{v}$ is nearly zero relative to Δv, or in other words, Δv is large. All other cases are insensitive, so that the closure in these cases is basically independent of the d_k^q. In (4.4) and (4.5), the Δv contribution to the relaxation terms is larger than the Δp

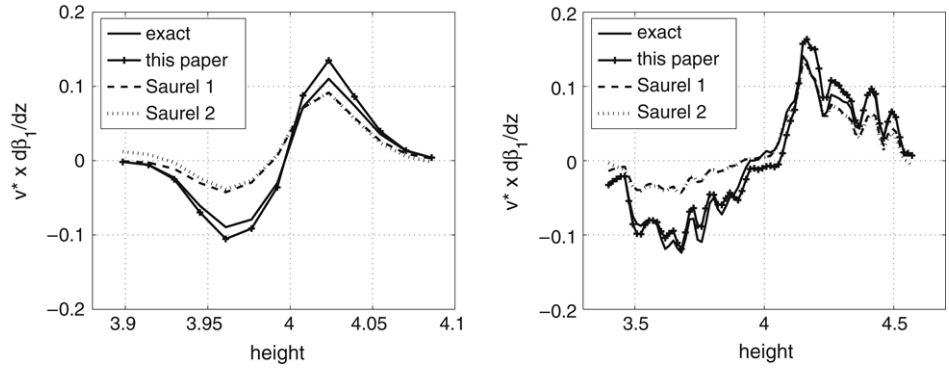

Fig. 3. The exact quantity $v^*\partial\beta_1/\partial z$ for the RT surface tension data set and the closed quantity $v^*\partial\beta_1/\partial z$ defined by (4.14) in the mixing zone at an early time, $t = 4$ (left) and a late time, $t = 9$ (right). We show closure of this paper and two interpretations of the closures of Saurel et al.

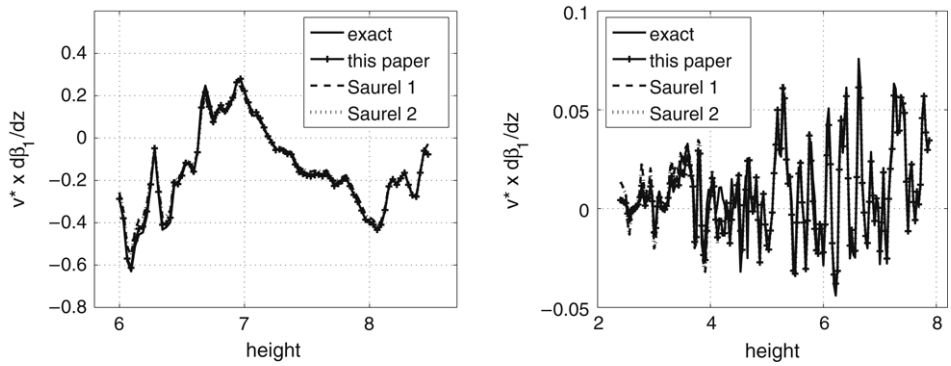

Fig. 4. The exact quantity $v^*\partial\beta_1/\partial z$ for the RM data set and closed quantity $v^*\partial\beta_1/\partial z$ defined by $d_k^v = 1$ in the mixing zone at $t = 35$ (left, after the first shock) and $t = 75$ (right, after reshock). We compare the closure from this paper and the closure of Saurel et al. The relaxation term is effectively zero, and has no effect on the closure, so that the two Saurel models coincide.

contribution, and as Δv occurs in the p^* relaxation, the p^* relaxation terms are generally significant while the v^* relaxation terms (proportional to Δp) are not.

When Δp is small, which is the case for all simulations considered here, including those with surface tension, $(pv)^* \approx p^*v^*$ is approximately independent of d_k^{pv}, which is thus insensitive to d_k^{pv}. However $(pv)^*$ is sensitive to v^*.

Our fifth main conclusion is the apparent insensitivity of the closures and averaged flow quantities to variation of (secondary) physics effects (ideal vs. surface tension vs. mass diffusion). These secondary mechanisms have a substantial influence on the growth rates of the mixing zone, i.e. α and the $Z_k(t)$. But once the influence of the edge motions has been scaled out of the data, the secondary physics appears to play only a small role in the simulation data, at least at length scales accessible at present levels of mesh refinement.

6. The v^* closure

The factor d_k^v in (4.11) is a ratio of logarithmic rates of volume creation for the two phases. The creation of volume arises primarily from the entrainment of previously unmixed (pure phase fluid) into the mixing zone [34] and also from the relative compression of the two fluids. We compare the exact and the closed expression for $v^*\partial\beta_1/\partial z$ in Figs. 3 and 4.

For the RT data set, we observe that the closure from this paper shows reasonable agreement with the data, and better than that of the Saurel closure. The relaxation terms have no affect on this comparison (see Fig. 3).

For the RM data set, we find full agreement (within the line width of the graphics) for both closures with the exact data (see Fig. 4). The agreement of the two closures can be ascribed to the facts that the closure convex coefficients μ_k^v in the present case are insensitive parameters and that the relaxation parameters are small.

7. The p^* closure

In the case of non-zero surface tension, pressure is discontinuous at the interface ∂X_k, and p_k is the value of the pressure defined by continuity from the interior of X_k. It is convenient to define

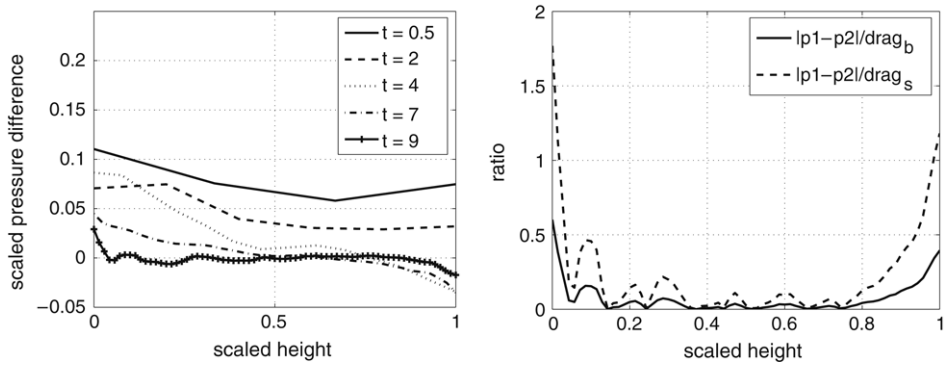

Fig. 5. Left: the scaled pressure difference $\Delta\tilde{p}/(Z_2 - Z_1)$ is plotted *vs.* the scaled height $(z - Z_1)/(Z_2 - Z_1)$ at $t = 0.5,\ 2,\ 4,\ 7,\ 9$ for the RT surface tension data. Right: the ratio of pressure difference and unit drag force $\rho_{k'}(\Delta v)^2/(Z_2 - Z_1)$ at $t = 9$.

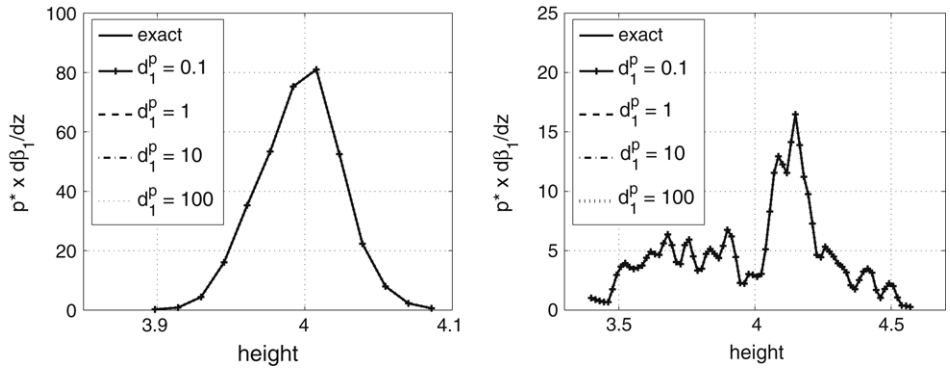

Fig. 6. The exact and the closed quantities $p^*\partial\beta_1/\partial z$ for four choices of d_k^p at $t = 4$ (left) and $t = 9$ (right). The curves are indistinguishable.

$$p^* = \frac{1}{2}(p_1^* + p_2^*), \tag{7.1}$$

and the capillary pressure

$$p_c^* = p_1^* - p_2^*, \tag{7.2}$$

so that

$$p_1^* = p^* + \frac{p_c^*}{2}, \qquad p_2^* = p^* - \frac{p_c^*}{2}. \tag{7.3}$$

p_c^* is the product of the surface tension σ and the average of the surface mean curvature. Similarly we define $(pv)^*$ and $(p_c v)^*$ as the average and the difference of the $(p_k v)^*$. We then define

$$\tilde{p_k} = p_k + (-1)^k \frac{p_c^*}{2} \tag{7.4}$$

$$\tilde{p_k^*} = p_k^* + (-1)^k \frac{p_c^*}{2} = p^*. \tag{7.5}$$

The required boundary condition (4.13) for p^* at the mixing zone edge Z_k can be reformulated as

$$\tilde{p_k} = \tilde{p_k^*} = p^* \quad \text{at } Z_k. \tag{7.6}$$

When the two fluids are mixing, their pressures tend to equilibrate. This equilibration is the mechanism whereby forces between the fluids are mediated. The equilibration is partial at early times, while at later times, a central portion of the mixing zone satisfies $\Delta\tilde{p} \approx 0$. This region of approximately complete equilibration increases and at late times it occupies most of the mixing zone, but in our data, it always excludes a region near the mixing zone edges. See Fig. 5 left frame, where we show pressure differences scaled by the mixing zone length. In the right frame, we scale this difference by a unit drag force. The conclusion is that the phase pressure differences are significant at the edges of the mixing zone.

The coefficient d_k^p represents a ratio of the forces accelerating the two fluids, each considered in the accelerated frame defined by their respective velocities [32]. The closure of p^* is insensitive to the choice of d_k^p. See Fig. 6. For definiteness, we

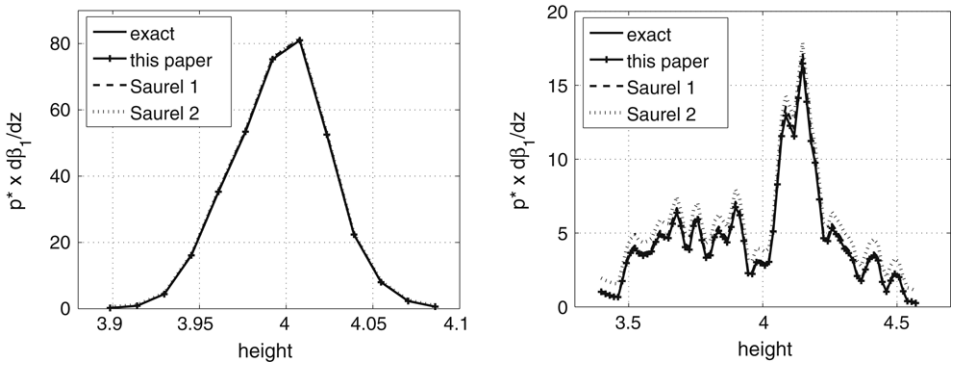

Fig. 7. The exact and closed quantities $p^*\partial\beta_1/\partial z$ for the RT surface tension data set at an early time, $t = 4$ (left) and a late time, $t = 9$ (right). We show one closure from this paper and two interpretations of the Saurel et al. closures.

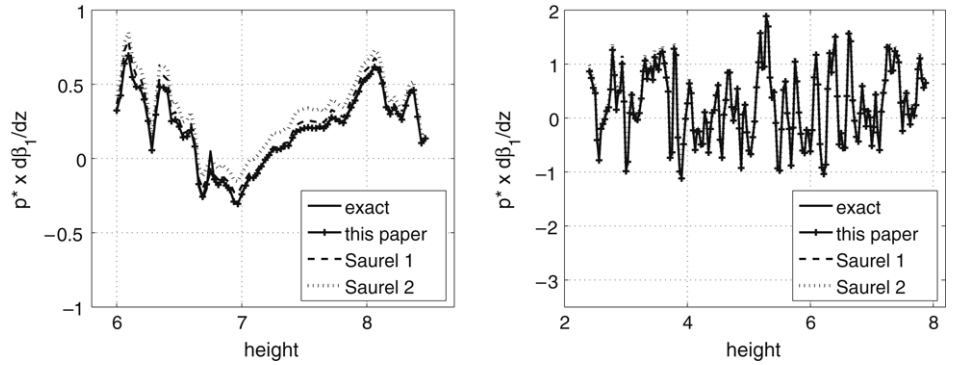

Fig. 8. The exact and closed quantities $p^*\partial\beta_1/\partial z$ for the RM data set at $t = 35$ (left, after the first shock) and $t = 75$ (right, after reshock). We show the closure from this paper and two interpretations of the Saurel et al. closures.

set $d_k^p = 1$. The exact quantity $p^*\partial\beta_1/\partial z$ and several closed expressions for the RT surface tension data set is plotted in Fig. 7. Note the degradation of the fit to data for the full Saurel closure (with relaxation) at late time.

For the RM data set, we compare the exact and the closed expression for $p^*\partial\beta_1/\partial z$ in Fig. 8. The two curves are indistinguishable.

The Saurel closure for the momentum equation is compared in Figs. 7 and 8 to the exact data and to the other closures. For both the RT and RM data sets, we observe that the fractional linear portion of the Saurel et al. closure fits well to the exact data at all time, while the complete closure shows some loss of agreement. The complete closure includes a relaxation effect proportional to $v_2 - v_1$, a quantity which is not small.

8. The $(pv)^*$ closure

In the case of non-zero surface tension, the work associated with limiting pressures is not continuous at the interface. We have

$$(p_1 v)^* - (p_2 v)^* = (p_c v)^*. \tag{8.1}$$

In Fig. 9, for RT surface tension data, we show that the closure is insensitive to the choice of the d_k^{pv}. Basically, the insensitivity results from the insensitivity to the choice of p^*. If $p_1 \approx p_2 \approx p^*$ then $(pv)^* \approx p^* v^*$ is independent of d_k^{pv}. For the RT surface tension data set, we compare the exact and closed expressions for $(pv)^*\partial\beta_1/\partial z$ in Fig. 10. We observe good performance for our closure. For RM mixing, the agreement with data is also excellent, see Fig. 11.

The Saurel closure for the energy equation is compared in Figs. 10 and 11 to the exact data and to the other closures. For the RT surface tension data, we find better agreement for our closure than for that of Saurel at early time and the reverse at late time. For the RM data set, we compare the exact and closed expressions for $(pv)^*\partial\beta_1/\partial z$ in Fig. 11. We observe that the fractional linear portion of the Saurel et al. closure fits well to the exact data at all time, while the complete closure is not as good at early time as the closures from this paper. All $(pv)^*$ deviation of the models from exact values are due to deviation in the v^* contribution to $(pv)^*$.

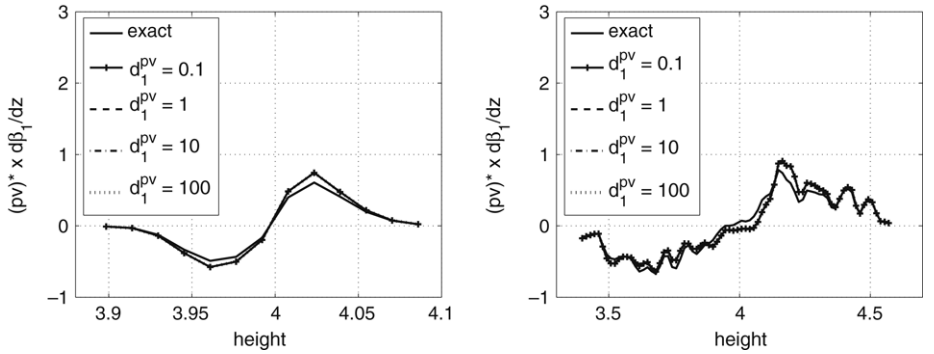

Fig. 9. The exact and closed quantities $(pv)^*\partial\beta_1/\partial z$ for the RT data set for four values of d_1^{pv} at early time, $t = 4$ (left) and at late time $t = 9$ (right).

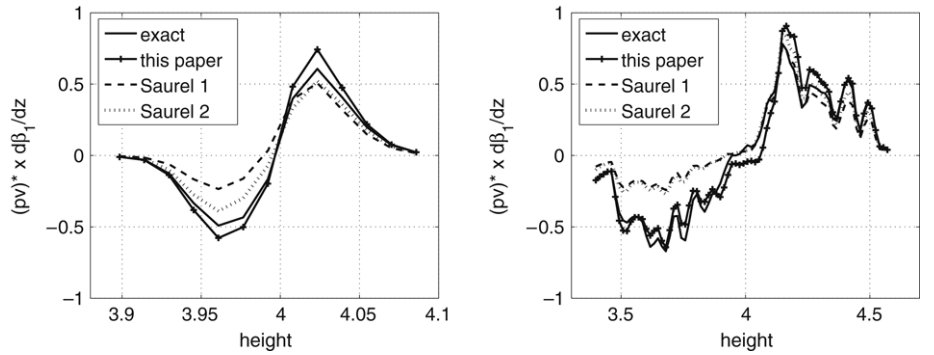

Fig. 10. The exact and closed quantities $(pv)^*\partial\beta_1/\partial z$ for the RT data set at early time, $t = 4$ (left) and at late time $t = 9$ (right). We show the closure from this paper and two interpretations of the Saurel et al. closures.

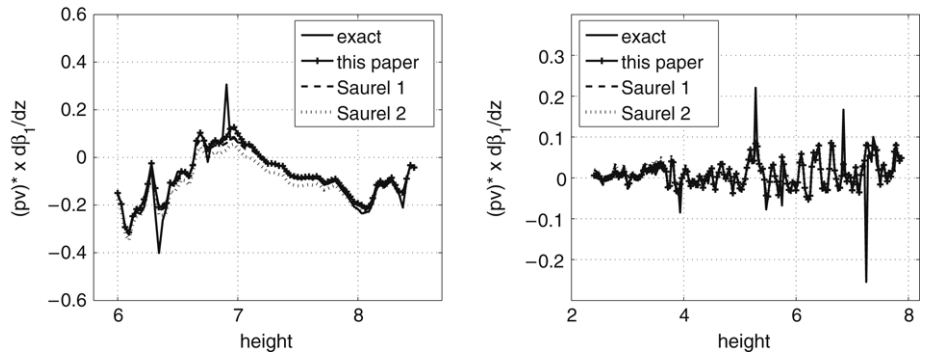

Fig. 11. The exact and closed quantities $(pv)^*\partial\beta_1/\partial z$ for the RM data set at $t = 35$ (left, after the first shock) and $t = 75$ (right, after reshock). We show one closure from this paper and two interpretations of the Saurel et al. closures.

9. Conclusions

The closures for v^*, p^* and $(pv)^*$ satisfy all required constraints of boundary conditions and conservation. The boundary constraints are given in (4.13). Phase k mass and (for rectangular geometry) total momentum are conserved in the absence of diffusion and viscosity (2.5) and (2.6). Total energy is conserved according to (2.7). Entropy should not be conserved because averaging is nonadiabatic, but an entropy inequality is enforced [33].

Comparison to simulation data shows excellent agreement for the closures. The p^* and $(pv)^*$ closure parameters are insensitive in this comparison, but the RT v^* parameters and the RT v^* contribution to $(pv)^*$ are sensitive. Comparison to an alternate closure shows reasonable but less satisfactory agreement, especially for the sensitive choices for the v^* closure and the v^* contribution to the $(pv)^*$ closure.

References

[1] P. Garabedian, On steady-state bubbles generated by Taylor instability, Proc. R. Soc. London A 241 (1957) 423–431.
[2] S. Chandrasekhar, Hydrodynamic and Hydromagnetic Stability, Oxford University Press, Oxford, 1961.
[3] D.H. Sharp, An overview of Rayleigh–Taylor instability, Physica D 12 (1984) 3–18.
[4] B. Cheng, J. Glimm, D.H. Sharp, Dynamical evolution of the Rayleigh–Taylor and Richtmyer–Meshkov mixing fronts, Phys. Rev. E 66 (2002) 1–7. paper No. 036312.
[5] D.L. Youngs, Numerical simulation of mixing by Rayleigh–Taylor and Richtmyer–Meshkov instabilities, Laser Part. Beams 12 (1994) 725–750.
[6] G. Dimonte, M. Schneider, Density ratio dependence of Rayleigh–Taylor mixing for sustained and impulsive acceleration histories, Phys. Fluids 12 (2000) 304–321.
[7] B. Cheng, J. Glimm, D.H. Sharp, Density dependence of Rayleigh–Taylor and Richtmyer–Meshkov mixing fronts, Phys. Lett. A 268 (2000) 366–374.
[8] B. Cheng, J. Glimm, D. Saltz, D.H. Sharp, Boundary conditions for a two pressure two phase flow model, Physica D 133 (1999) 84–105.
[9] B. Keyfitz, Admissibility conditions for shocks in conservation laws that change type, SIAM J. Math. Anal. 22 (1991) 1284–1292.
[10] B. Cheng, An overview of mix models, in: M. Legrand, M. Vandenboomgaerde (Eds.), Proceedings of the tenth international workshop on the physics of compressible turbulent mixing, Commissariat a l'Energie Atomique, 2007.
[11] E. George, J. Glimm, X.L. Li, Y.H. Li, X.F. Liu, The influence of scale-breaking phenomena on turbulent mixing rates, Phys. Rev. E 73 (2006) 016304–1–016304–5.
[12] X.F. Liu, E. George, W. Bo, J. Glimm, Turbulent mixing with physical mass diffusion, Phys. Rev. E 73 (2006) 056301–1–056301–8.
[13] J. Glimm, H. Jin, M. Laforest, F. Tangerman, Y. Zhang, A two pressure numerical model of two fluid mixing, Multiscale Model. Simul. 1 (2003) 458–484.
[14] W. Bo, H. Jin, D. Kim, X. Liu, H. Lee, N. Pestieau, Y. Yan, J. Glimm, J. Grove, Multi phase closure models, Stony Brook University, Preprint Number SUNYSB-AMS-07-02.
[15] B. Cheng, J. Glimm, D.H. Sharp, Y. Yu, A multiphase flow model for the unstable mixing of layered incompressible materials, Phys. Fluids 17 (2005) 087102–1–07102–8, paper No. 087102. LANL Preprint Number LA-UR-05-0078. Stony Brook University Preprint Number SUNYSB-AMS-05-01.
[16] D.A. Drew, Mathematical modeling of two-phase flow, Ann. Rev. Fluid Mech. 15 (1983) 261–291.
[17] L. Malvern, Introduction to the Mechanics of Continuous Medium, Prentice Hall, 1969.
[18] Y. Chen, Two phase flow analysis of turbulent mixing in the Rayleigh–Taylor instability, Ph.D. Thesis, University at Stony Brook, 1995.
[19] Y. Chen, J. Glimm, D.H. Sharp, Q. Zhang, A two-phase flow model of the Rayleigh–Taylor mixing zone, Phys. Fluids 8 (3) (1996) 816–825.
[20] D. Saltz, D. Sendersky, Computation of two-phase mixing properties in Rayleigh–Taylor instability, Tech. Rep., University at Stony Brook, 1999.
[21] R. Bird, W. Stewart, E. Lightfoot, Transport Phenomena, second edn, John Wiley & Sons, New York, 2002.
[22] K.I. Read, Experimental investigation of turbulent mixing by Rayleigh–Taylor instability, Physica D 12 (1984) 45–58.
[23] V.S. Smeeton, D.L. Youngs, Experimental investigation of turbulent mixing by Rayleigh–Taylor instability (part 3), AWE Report Number 0 35/87, 1987.
[24] A. Banerjee, M.J. Andrews, Statistically steady measurements of Rayleigh–Taylor mixing in a gas channel, Phys. Fluids 18 (3) (2006) 35107–1–35107–13.
[25] G. Dimonte, D.L. Youngs, A. Dimits, S. Weber, M. Marinak, S. Wunsch, C. Garsi, A. Robinson, M. Andrews, P. Ramaprabhu, A.C. Calder, B. Fryxell, J. Bielle, L. Dursi, P. MacNiece, K. Olson, P. Ricker, R. Rosner, F. Timmes, H. Tubo, Y.-N. Young, M. Zingale, A comparative study of the turbulent Rayleigh–Taylor instability using high-resolution three-dimensional numerical simulations: The alpha-group collaboration, Phys. Fluids 16 (2004) 1668–1693.
[26] W. Cabot, A. Cook, Reynolds number effects on Rayleigh–Taylor instability with possible implications for type Ia supernovae, Nature Phys. 2 (2006) 562–568.
[27] Y. Yu, M. Zhao, T. Lee, N. Pestieau, W. Bo, J. Glimm, J.W. Grove, Uncertainty quantification for chaotic computational fluid dynamics, J. Comp. Phys. 217 (2006) 200–216, Stony Brook Preprint number SB-AMS-05-16 and LANL preprint number LA-UR-05-6212.
[28] R. Courant, K. Friedrichs, Supersonic Flow and Shock Waves, Springer-Verlag, New York, 1967.
[29] R. Saurel, R. Abgrall, A multiphase Godunov method for compressible multifluid and multiphase flows, J. Comput. Phys. 150 (1999) 425–467.
[30] R. Abgrall, R. Saurel, Discrete equations for physical and numerical compresible multiphase mixtures, J. Comput. Phys. 186 (2003) 361–396.
[31] A. Chinnayya, E. Daniel, R. Saurel, Modelling detonation waves in heterogeneous energetic materials, J. Comput. Phys. 196 (2004) 490–538.
[32] H. Jin, J. Glimm, D.H. Sharp, Compressible two-pressure two-phase flow models, Phys. Lett. A 353 (2006) 469–474.
[33] H. Jin, J. Glimm, D.H. Sharp, Entropy of averaging for compressible two-pressure two-phase models, Phys. Lett. A 360 (2006) 114–121, Stony Brook University Preprint number SUNYSB-AMS-06-08 and Los Alamos National Laboratory.
[34] J. Glimm, D. Saltz, D.H. Sharp, Two-pressure two-phase flow, in: G.-Q. Chen, Y. Li, X. Zhu (Eds.), Nonlinear Partial Differential Equations, World Scientific, Singapore, 1998, pp. 124–148.
[35] J. Glimm, D. Saltz, D.H. Sharp, Renormalization group solution of two-phase flow equations for Rayleigh–Taylor mixing, Phys. Lett. A 222 (1996) 171–176.
[36] J. Glimm, D. Saltz, D.H. Sharp, Two-phase modeling of a fluid mixing layer, J. Fluid Mech. 378 (1999) 119–143.
[37] B. Cheng, J. Glimm, D.H. Sharp, A 3-D RNG bubble merger model for Rayleigh–Taylor mixing, Chaos 12 (2002) 267–274.
[38] H. Jin, X.F. Liu, T. Lu, B. Cheng, J. Glimm, D.H. Sharp, Rayleigh–Taylor mixing rates for compressible flow, Phys. Fluids 17 (2005) 024104–1–024104–10.
[39] E. George, J. Glimm, Self similarity of Rayleigh–Taylor mixing rates, Phys. Fluids 17 (2005) 054101–1–054101–13, Stony Brook University Preprint number SUNYSB-AMS-04-05.